DOI：10. 11835/j. issn. 2096-6717. 2024. 024

开放科学(资源服务)标识码 OSID:

Machine learning-based investigation of uplift resistance in special-shaped shield tunnels using numerical finite element modeling

ZHANG Wengang[1a,1b,1c], *YE Wenyu*[1a], *SUN Weixin*[1a], *LIU Zhicheng*[2], *LI Zhengchuan*[3]

(1a. Key Laboratory of New Technology for Construction of Cities in Mountain Area, Ministry of Education; 1b. School of Civil Engineering; 1c. National Joint Engineering Research Center of Geohazards Prevention in the Reservoir Areas, Chongqing University, Chongqing 400045, P. R. China; 2. Guangzhou Metro Group Co., LTD., Guangzhou 510010, P. R. China; 3. CREEC(Chongqing) Survey, Design and Research Co., Ltd., Chongqing 400023, P. R. China)

Abstract: The uplift resistance of the soil overlying shield tunnels significantly impacts their anti-floating stability. However, research on uplift resistance concerning special-shaped shield tunnels is limited. This study combines numerical simulation with machine learning techniques to explore this issue. It presents a summary of special-shaped tunnel geometries and introduces a shape coefficient. Through the finite element software, Plaxis3D, the study simulates six key parameters—shape coefficient, burial depth ratio, tunnel's longest horizontal length, internal friction angle, cohesion, and soil submerged bulk density—that impact uplift resistance across different conditions. Employing XGBoost and ANN methods, the feature importance of each parameter was analyzed based on the numerical simulation results. The findings demonstrate that a tunnel shape more closely resembling a circle leads to reduced uplift resistance in the overlying soil, whereas other parameters exhibit the contrary effects. Furthermore, the study reveals a diminishing trend in the feature importance of buried depth ratio, internal friction angle, tunnel longest horizontal length, cohesion, soil submerged bulk density, and shape coefficient in influencing uplift resistance.

Keywords: special-shaped tunnel; shield tunnel; uplift resistance; numerical simulation; machine learning

基于数值模拟和机器学习的异形盾构隧道抗隆起性能研究

仉文岗[1a,1b,1c],叶文煜[1a],孙伟鑫[1a],刘智成[2],李正川[3]

(1. 重庆大学 a. 山地城镇建设与新技术教育部重点实验室; b. 土木工程学院; c. 库区环境地质灾害防治国家地方联合工程研究中心,重庆 400045; 2. 广州地铁集团有限公司,广州 510010; 3. 中铁二院重庆勘察设计研究院有限公司,重庆 400023)

Received: 2024-02-21

Foundation items: Guangzhou Metro Scientific Research Project (No. JT204-100111-23001); Chongqing Municipal Special Project for Technological Innovation and Application Development (No. CSTB2022TIAD-KPX0101); Science and Technology Research and Development Program of China State Railway Group Co., Ltd. (No. N2023G045)

Author brief: ZHANG Wengang (1983-), PhD, professor, main research interest: geotechnical engineering, E-mail: cheungwg@126.com.

SUN Weixin (corresponding author), PhD candidate, E-mail: weixins@cqu. edu. cn.

摘 要:覆土盾构隧道的土壤抗浮力对其防浮稳定性有重要影响,目前关于异形盾构隧道的抗浮研究还比较有限。采用数值模拟结合机器学习研究异形盾构隧道的抗浮特性,总结异形盾构隧道的几何形态,引入形状系数,利用Plaxis3D有限元软件,开展形状系数、埋深比、隧道最长水平长度、内摩擦角、黏聚力和土壤浸没体积密度6个关键参数的模拟,研究这6个参数在不同条件下对抗浮力的影响;采用XGBoost和ANN机器学习方法,基于数值模拟结果分析各参数的特征重要性。结果表明,覆土的抗浮力随隧道形状接近圆形而降低,其他参数呈现出相反的趋势;埋深比、内摩擦角、隧道最大水平长度、黏聚力、土壤浸没体积密度和形状系数在影响抗浮力方面的特征重要性呈现递减趋势。

关键词:异形隧道;盾构隧道;抗浮力;数值模拟;机器学习

中图分类号:U456.3 **文献标志码**:A **文章编号**:2096-6717(2026)01-0001-13

1 Introduction

The demand for efficient transportation networks, urban development, and utility infrastructure has resulted in a surge of underground construction projects worldwide. The tunneling shield technique was a groundbreaking innovation that revolutionized the excavation and construction of underground tunnels[1]. Its applications span an extensive spectrum of infrastructure projects like metro systems, road and railway tunnels, water conveyance tunnels, and utility networks. These machines offer compelling advantages, including heightened construction efficiency, minimized environmental disturbances, elevated safety and stability standards, as well as cost-effectiveness. However, as the utilization of underground space started to increase, conventional circular shield machines could no longer adequately cater to the escalating market requirements[2]. Consequently, there is a growing trend towards designing and deploying special-shaped shield machines tailored to specific project needs. Currently, special-shaped shield machines applied in civil engineering predominantly comprise sub-rectangular[3-6], quasi-rectangular[7-10], and rectangular shield machines[11-14]. While the above equipment and methods play a crucial role in underground transportation construction projects, further in-depth research is still necessary to enhance the safety of shield tunnel construction and operation.

During shield tunnel construction, various challenges may arise, with the floating of shield tunnels being one of the most common problems. To address this issue, multiple methods have been developed to control the buoyancy of shield tunnels. These encompass drainage and pressure reduction[15], grouting reinforcement[16], and optimizing soil overburden thickness[17-18]. Numerous scholars have conducted research on the thickness and uplift resistance of the overlying soil above shield tunnels. White et al. [19-20] employed centrifuge simulations on the uplift failure of sandy soil and further explored the failure behavior of sand overlying underground structures experiencing uplift. Subsequent studies by Gong et al. [21] and Robert & Thusyanthan[22] employed transparent soil models and numerical simulations, respectively, to examine the uplift resistance variation in soil over circular underground structures. Extending the understanding of soil deformation mechanisms, Guo et al. [17] and Liu et al. [23]developed distinct methods for determining the shallowest soil thickness of shield tunnels in clay and sand layers, respectively, using the limit equilibrium method. However, the existing research exclusively focuses on traditional circular shield tunnels, which is inadequate for calculating uplift resistance in special-shaped shield tunnels and designing appropriate overlying soil thickness. Special-shaped tunnels, as opposed to their traditional circular counterparts, exhibit distinct mechanical behaviors, particularly in terms of buoyancy resistance. This divergence primarily stems from the unique geometrical configurations of special-shaped tunnels, which influence the distribution and magnitude of stresses within the surrounding soil. Consequently, there is a critical need for further exploration in this domain.

In addition, traditional research methods face difficulties when analyzing the relationship between soil behavior and infrastructure structures in geotechnical engineering. However, the integration of nu-

merical simulation and machine learning techniques offers a promising avenue to overcome these constraints, as highlighted by Zhang et al. [24] This combination enhances the understanding, prediction, and optimization of geotechnical processes, thus leading many scholars to adopt this approach in their research. These studies encompass a broad spectrum of research issues, including tunnel uplift induced by liquefaction[25], basement uplift[26] resulting from excavation of foundation pits in anisotropic soil, and the soil parameters influencing undrained shear strength in soft clay[27]. Furthermore, Liu et al. [28-29] proposed the utilization of machine learning in landslide research using a methodological approach that fuses mathematical and physical aspects to scrutinize landslide susceptibility.

This study aims to analyze the uplift resistance of the soil overlying special-shaped shield tunnels in practical engineering. We consider various instances of special-shaped shield tunnels and introduce a value modulus model encompassing multiple parameter variables. By integrating machine learning techniques and utilizing the outcomes of numerical simulations, we analyze the key variables that influence the uplift resistance of the soil above these unique shield tunnels.

2　Basic theory

2.1　Analysis of the floating mechanism

The factors contributing to shield tunnel uplift can be classified into three categories according to different stages[30]. The first category emerges during the excavation stage, when the soil undergoes unloading because the overall weight of the tunnel lining is lower than that of the excavated soil block. Consequently, a slight uplift occurs in the shield tunnel due to ground stress (as depicted in Fig. 1(a)). As in-situ stress redistributes, the tunnel structure gradually stabilizes. Commonly, soil reinforcement and sequential excavation methods are employed during this phase to offer support to shield tunnels, with the objective of minimizing ground movement and uplift effects.

The other two factors leading to tunnel buoyancy are grouting pressure and groundwater buoyancy,

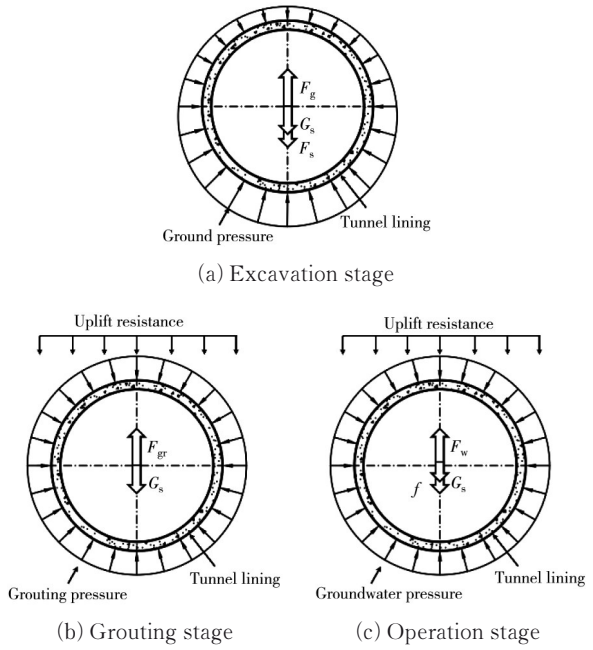

Note: F_g is the buoyancy caused by soil excavation; G_s is the weight of tunnel lining; F_s is the additional support force; F_{gr} is the buoyancy provided by grouting slurry; F_w is the buoyancy exerted by groundwater; f is the friction between tunnel lining and surrounding soil.

Fig. 1　Schematic diagram of the forces during the floating stage of the shield tunnel

encountered during the grouting stage and operational stage, respectively (as illustrated in Fig. 1(b) & (c)). Mitigating tunnel buoyancy during these stages involves designing the thickness of the soil covering the tunnel[23]. The basic concept is that the overlying soil provides uplift resistance, counterbalancing buoyancy and surpassing the tunnel lining's self-weight and the friction between the tunnel and the surrounding soil. With increasing tunnel depth, the uplift resistance capacity provided by the overlying soil also increases, thereby enhancing the anti-buoyancy stability of the shield tunnel.

2.2　Research on uplift resistance

The uplift resistance of overlying soil on underground structures results from the combined effect of structure weight and shear force between the disturbed soil and its surroundings. Numerous scholars have investigated the uplift resistance magnitude for circular underground structures (as shown in Table 1), yet diverse calculation methods are employed due to variations in selected sliding surfaces and assumed conditions. Notably, research has been primarily confined to circular structures, neglecting the impact of special-shaped geometries on uplift resistance.

Table 1 Predictive-analytical models

Reference	Soil type	Reference	Soil type	Reference	Soil type
Vermeer and Sutjiadi. 1985[31]	CL	Schaminée et al. 1990[32]	CL,C	Palmer et al. 2003[34]	CL
White et al. 2001[19]	CL	White et al. 2008[20]	CL	Magda et al. 2000[35]	CL
Liu et al. 2015[23]	CL	Ng et al. 2006[33]	CL	Gong et al. 2018[21]	C
Guo et al. 2021[18]	CL,C	Guo et al. 2018[17]	CL,C	Sun et al. 2023[36]	CL

Notes: CL denotes cohesionless soil; C denotes cohesive soil.

3 Application of special-shaped shield tunnels

Shield tunnels can be categorized into four main types based on their cross-sectional shape: circular [17-18], quasi-rectangular shield [7-10], sub-rectangular [3-6], and rectangular [11-14]. The present study aims to investigate the uplift resistance of the overlying soil in these four types of shield tunnels. This section is an introduction to these shield tunnel types, their distinctive characteristics, significance in underground construction and transportation infrastructure, and their implications for geotechnical engineering.

3.1 The circular shield tunnel

The circular shield tunnel stands as one of the most traditional and widely used cross-sectional shapes in tunneling projects. Its shape provides excellent structural stability, rendering it suitable for a wide range of ground conditions. Notably, circular tunnels are particularly favored in soft ground and cohesive soils due to their uniform stress distribution and relatively straightforward excavation process. Moreover, the circular cross-section effectively minimizes the risk of ground settlement and ensures robust load-bearing capabilities. Circular shield tunnels find diverse engineering applications, evidenced by numerous significant projects. For instance, a circular shield tunnel with an outer diameter of 6 m was utilized between Chaoyang Station and Zaoying Station of Beijing Subway No. 14. Additionally, Hefei Metro Line 3 employed circular shield tunnels for the section stretching from Qimen Road Station to Grand Theater Station[18].

3.2 The quasi-rectangular shield tunnel

The quasi-rectangular shield tunnel presents a hybrid cross-sectional shape that combines features of circular and rectangular designs. Noteworthy for its rounded corners, which emulate a modified rectangular profile, this configuration aspires to strike a balance between the advantages offered by circular and rectangular tunnels. As a result, it delivers enhanced space utilization and elevated load-bearing capacity, rendering it a fitting choice for diverse engineering endeavors. The quasi-rectangular shield tunnel finds application in various scenarios, including its utilization in the soft clay context of Ningbo Metro Line 3[7,9]. Moreover, Ding et al. [10] conducted experimental investigations into the structural attributes of quasi-rectangular shield tunnels, while Li et al. [8] employed numerical simulations to analyze their behavior.

3.3 The sub-rectangular shield tunnel

The sub-rectangular shield tunnel refers to a cross-sectional shape with elongated sides and rounded corners, resembling a horizontally stretched rectangle. This configuration is often utilized in tunnel projects where the available space allows for a broader and shallower profile. The sub-rectangular design provides increased flexibility for accommodating larger transportation infrastructure, such as subway lines or utility corridors. In the Shanghai area, the construction of sub-rectangular shield tunnels has been explored in several studies, including those conducted by Zhu et al. [4], Pham et al. [5], and Do et al. [6]. Additionally, Huang et al. [3] conducted a full-scale experimental research on a newly designed sub-rectangular shield tunnel.

3.4 The rectangular shield tunnel

The rectangular shield tunnel features a straight and elongated cross-sectional shape, offering maximum usable space compared to other designs. Its configuration makes it well-suited for accommodating large-scale transportation infrastructure and utility systems, providing ample room for tracks, roadways, or various services. Noteworthy examples of the engineering applications of rectangular shield tunnels include the Kyoto Subway Tozai Line in Japan from October 1, 1999 to October 31, 2003 [12], the

rectangular pipe gallery tunnel near the intersection of Chengbeidong Road and Qimen Interchange in Suzhou, China[11], and the rectangular tunnel under Hongzhuan Road by the China Railway Engineering Group in 2003[13].

4 Numerical finite element analysis

In light of the limited existing research concerning the uplift resistance of overlying soil in special-shaped shield tunnels, this section seeks to address this knowledge gap by utilizing the Plaxis3D finite element numerical simulation software.

4.1 Research project

4.1.1 Shape coefficient of special-shaped shield tunnel

To analyze the effect of tunnel shape on uplift resistance, we propose a shape coefficient for special-shaped shield tunnels. As depicted in the figure below, a circle is inscribed with the longest axis in the tunnel section as the diameter ($2R_c$), and the center of the tunnel serves as the origin. The special-shaped tunnel's shape coefficient is defined as the ratio of the enclosed area of the tunnel section (A_t), as illustrated by Eq. (1) and depicted in Fig. 2. A value close to 1 indicates a more circular tunnel section, whereas values deviating further from 1 signify a departure from circular geometry.

$$\eta = \frac{A_t}{\pi R_c^2} \tag{1}$$

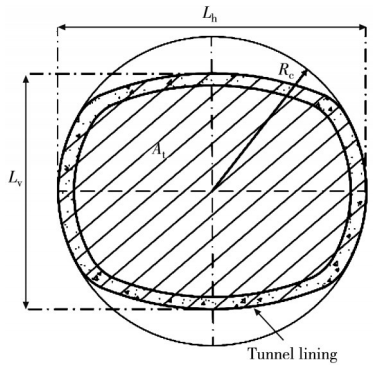

Note: L_h is the longest horizontal length of the cross-section of the shield tunnel; L_v is the longest vertical length of the cross-section of the shield tunnel.

Fig. 2　Schematic diagram of the definition of shape coefficient for special-shaped shield tunnels

4.1.2 Selection of shape for special-shaped shield tunnel

The strategy for defining tunnel shapes in this study is based on the research conducted by Do et al. [6]. The geometric configurations of the four tunnel types share certain similarities. Specifically, when the lengths of the two symmetrical axes of the quasi-rectangular tunnel and the sub-rectangular tunnel are equal, these shapes lie between a circle and a rectangle. Consequently, the shapes of the circular, quasi-rectangular, sub-rectangular, and rectangular shield tunnels exhibit a gradual transition from a circle to a rectangle.

To establish the tunnel shapes, the initial dimensions of the tunnel in Zhu et al. [4] (2019)'s research are utilized. They consist of a long and a short axes measuring 10.7 m × 8.2 m, respectively. The conditions for tunnel shape variation are achieved by shortening the length of the long axis while keeping constant the short axis. Furthermore, due to the unique geometry of circular tunnels, the method of equal difference variation is employed to modify tunnel diameter. Fig. 3 displays shield tunnels of varying shapes along with their respective geometric parameters utilized in this study.

4.1.3 Numerical simulation verification and research scheme

The numerical simulation method is a commonly employed research technique in geotechnical engineering to analyze the influential parameters affecting the uplift resistance of the overlying soil above tunnels. The numerical simulation model undergoes initial validation against previous research's measurement data on uplift resistance. Based on the datasets from various references, Fig. 4 shows the shape coefficient of irregular shield tunnels along the x-axis, while the y-axis represents the normalized uplift resistance.

The soil parameters chosen to investigate the influence of uplift resistance on the overlying soil of special-shaped shield tunnels are derived from prior research. Liu et al. [23] and Sun et al. [36] have proposed that uplift resistance demonstrates both nonlinear and linear growth trends concerning the increase in soil weight and internal friction angle, respectively. Furthermore, Guo et al. [17] (2018)'s findings suggest that the presence of cohesive force positively impacts uplift resistance. As discussed in the preceding section, the dimensions and shape of the tunnel may also influence the uplift force. Hence, three tunnel

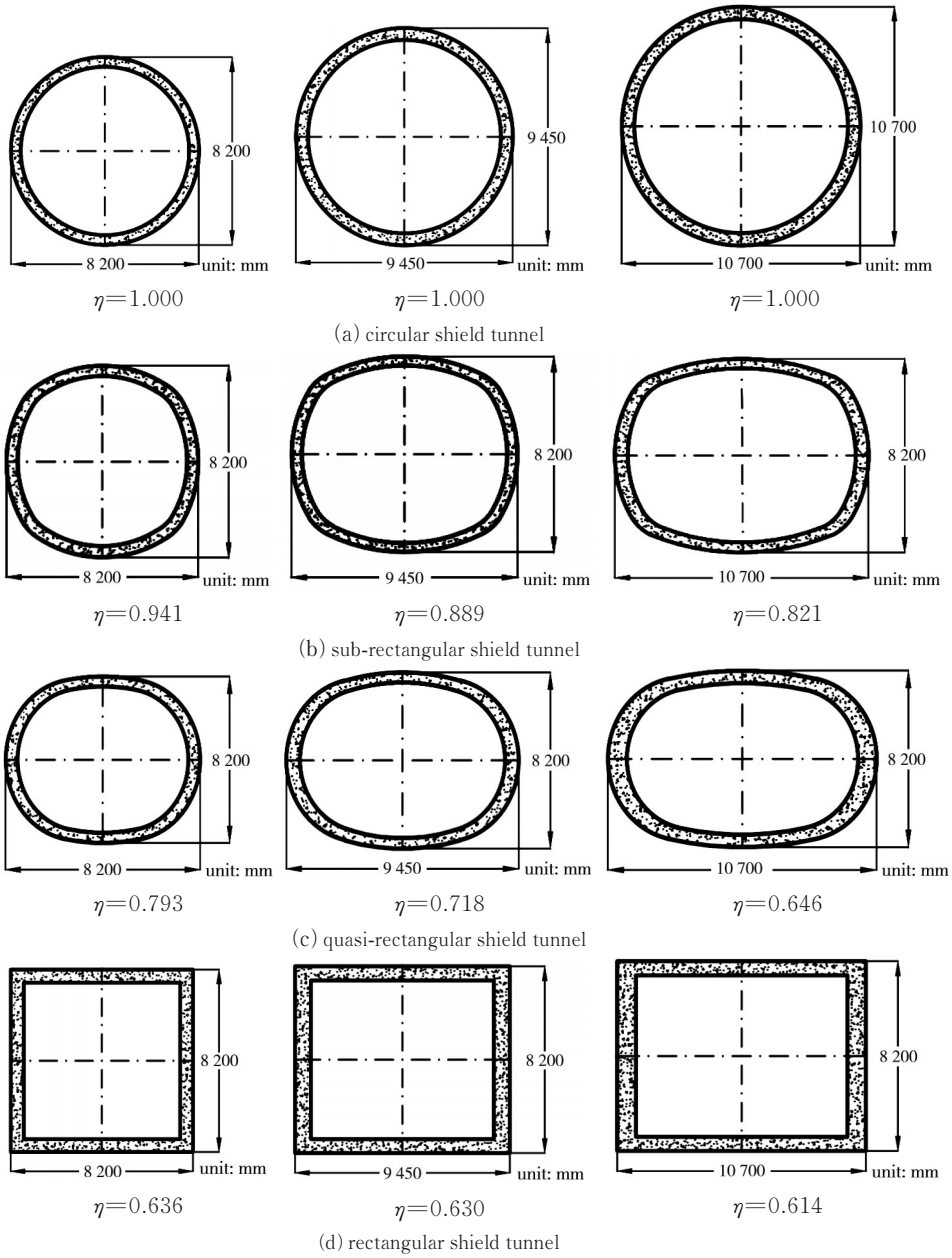

Fig. 3 Shapes for special-shaped shield tunnels

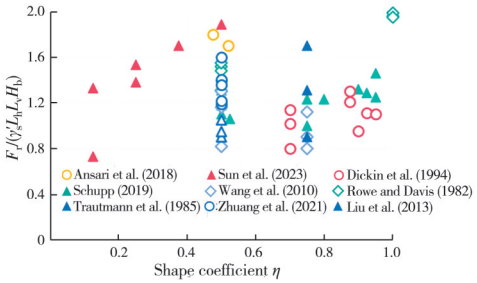

Fig. 4 Measurement data of normalized uplift resistance

geometric parameters, namely burial depth ratio, shape coefficient, and longest horizontal length, are selected for further examination, as shown in Table 2.

4.2 Numerical modeling

The numerical simulation comprises soil layer and tunnel structures. The Mohr-Coulomb model is employed to simulate soil behavior, with corresponding soil parameters input (as shown in Table 2). A linear elastic model is used to simulate the tunnel lin-

Table 2 Modeling parameters

Soil parameters			Tunnel parameters		
Cohesion c/kPa	Internal friction angle φ/(°)	Soil submerged bulk density γ_s'/(kN/m^3)	Burial depth ratio H_b/L_r	Shape coefficient η	Longest horizontal length L_h/m
0, 10, 20	10, 20, 30	6, 8, 10	0.50, 1.00, 1.50	1.000, 0.941, 0.889, 0.821, 0.793, 0.718, 0.646, 0.636, 0.630, 0.614	8.20, 9.45, 10.70

ing. The model's bottom is fixed with constraints, the surroundings are subjected to normal constraints, and the top is set with free constraints. To mitigate boundary effects, the model size shown in Fig. 5 is employed for modeling.

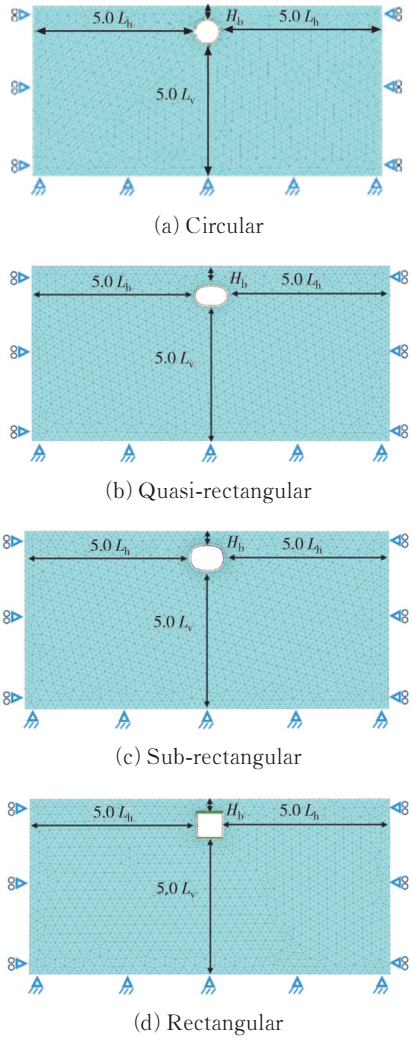

(a) Circular

(b) Quasi-rectangular

(c) Sub-rectangular

(d) Rectangular

Fig. 5　Numerical model mesh

The tunnel model is established using the tunnel generator function in Plaxis3D, and a tunnel lining structure is generated by importing CAD-drawn geometric shapes of a special-shaped shield tunnel.

The simulation and calculation procedure employed to assess the uplift resistance of soil above a special-shaped shield tunnel is outlined as follows:

(1) Initial alignment of the soil layer and tunnel geometry with the designated design plan.

(2) Establishment of geostress balance, denoted as K_0 balance, as the preliminary step.

(3) Simulation of the soil excavation process and activation of the tunnel within the model.

(4)Application of controlled upward vertical displacement to the tunnel model, with continuous recording of the relationship between the uplift resistance of the overlying soil and the displacement. Notably, as illustrated in Fig. 6, a point is reached where the uplift resistance starts diminishing with the progressive increase in vertical displacement. This critical point is where the uplift resistance provided by the overlying soil reaches its maximum [19-20].

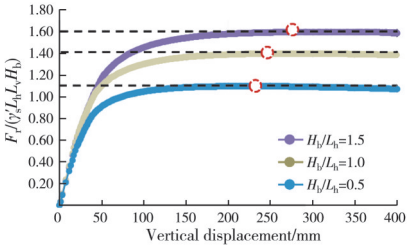

Fig. 6　Uplift resistance changes with vertical displacement
($\eta = 1.0$, $\gamma'_s = 6$ kN/m^3, $\varphi = 10°$, $c = 10$ kPa)

4.3　Results and analyses

Fig. 7 shows a comparison between the normalized uplift resistance of the tunnel overlying soil as determined through numerical simulation and the corresponding monitoring data extracted from prior studies. With a coefficient of determination (R^2) of 0.817 7 for both datasets, the results underscore the accuracy of the numerical model proposed in this research to anticipate the uplift resistance of tunnels. Based on the numerical model, simulate the conditions in Table 2.

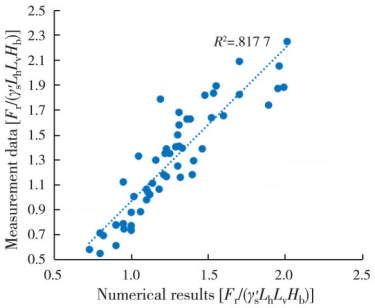

Fig. 7　Comparison between the model-predicted values and centrifuge results

This section presents an analysis of the impact of six parameters—shape coefficient, burial depth ratio, tunnel's longest horizontal length, internal friction angle, cohesion, and soil submerged bulk density—on uplift resistance magnitude using partial numerical simulation results. Fig. 8 shows that, apart from the tunnel shape coefficient, which reduces uplift resistance, all other parameters exhibit a positive correlation with uplift resistance. A more circular

tunnel shape (with a shape coefficient closer to 1) results in lower uplift resistance from the soil covering the tunnel. Additionally, increasing the tunnel's longest horizontal length leads to higher uplift resistance of the overlying soil (as shown in Fig. 8(e)).

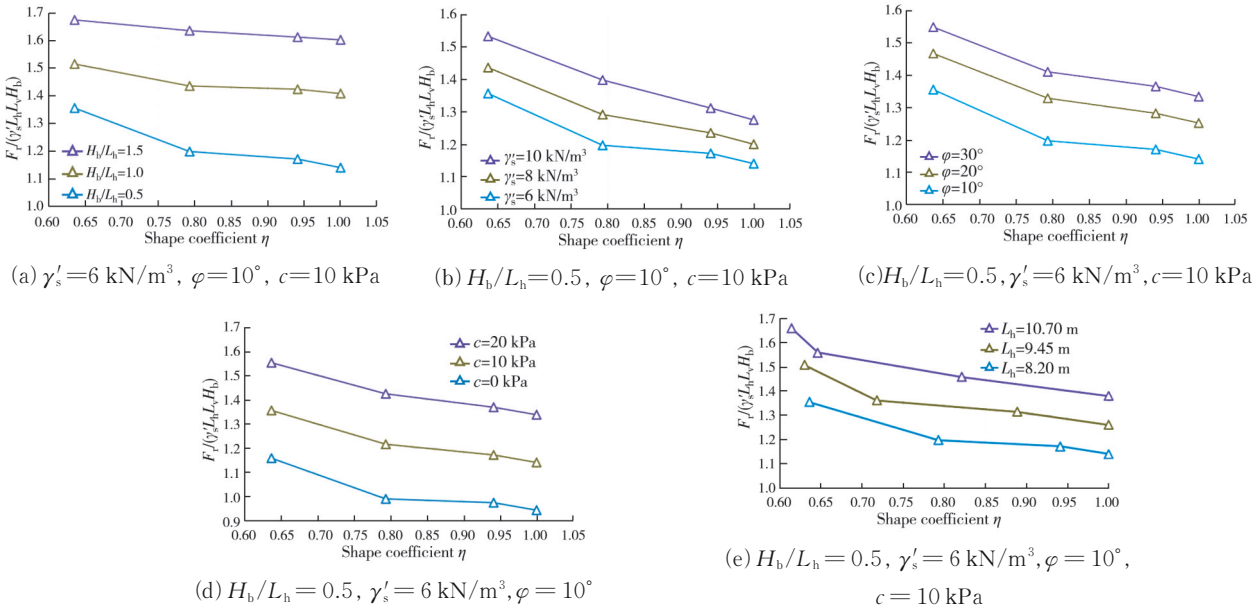

(a) γ'_s=6 kN/m³, φ=10°, c=10 kPa (b) H_b/L_h=0.5, φ=10°, c=10 kPa (c) H_b/L_h=0.5, γ'_s=6 kN/m³, c=10 kPa

(d) H_b/L_h=0.5, γ'_s=6 kN/m³, φ=10° (e) H_b/L_h=0.5, γ'_s=6 kN/m³, φ=10°, c=10 kPa

Fig. 8 Variation of normalized uplift resistance with parameters

In the scope of tunnel shape coefficients explored within this study, subtle variations are observed in the impact of burial depth ratio, soil submerged bulk density, internal friction angle, and cohesion on uplift force. Specifically, increasing the burial depth ratio of the soil from 0.5 to 1.0 and 1.5 yields uplift resistance increments ranging from 1.12 to 1.22 and 1.24 to 1.39, respectively. Similarly, raising the submerged bulk density of the soil from 6 to 8 and 10 corresponds to uplift resistance increases within the range of 1.04 to 1.06 and 1.11 to 1.13, respectively. Additionally, notable changes in uplift resistance occur as the internal friction angle increases from 10° to 20° and 30°, resulting in increments of 1.08 to 1.10 and 1.14 to 1.16, respectively. Notably, variations in cohesion, ranging from 10 to 0 and subsequently increasing to 20, induce changes in uplift resistance within the range of 0.80 to 0.85 and 1.15 to 1.16, respectively. These findings provide critical insights into the complex interplay between the examined parameters and the resulting uplift resistance.

5 Prediction models for uplift resistance

In this research, machine learning methods, specifically XGBoost and Artificial Neural Networks (ANN), were employed to construct robust predictive models to forecast uplift resistance based on the provided input parameters. Moreover, the feature importance of each parameter will be examined using these models to understand their relative contributions to the tunnel uplift resistance.

5.1 Dataset

The six parameters along with their corresponding value ranges, as presented in Table 2, are utilized in this study for predicting uplift resistance and conducting a thorough analysis of parameter importance. With these parameters and their respective value ranges, numerical simulation results are obtained through comprehensive simulations. The uplift resistance values derived from these simulations serve as the dependent variable for the prediction models.

Fig. 9 displays the correlation heat map of the feature variables, generated from the numerical simulation scheme. This visualization succinctly represents the interrelationships among these variables. The numerical values in the correlation heat map indicate the degree and trend of correlation between pairs of feature variables. Values closer to −1 or 1 indicate a robust correlation, whereas those close to 0 suggest a weak or negligible correlation. Notably,

the variables in this study exhibit minimal correlation. Therefore, machine learning methods appear more suitable to evaluate the impact of these variables on uplift resistance.

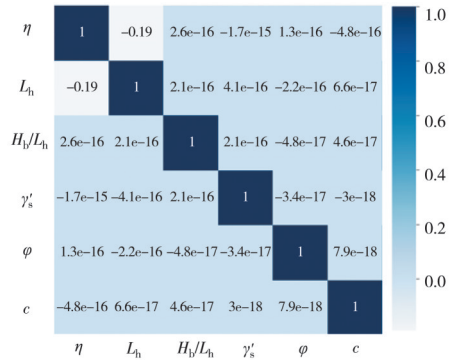

Fig. 9　Correlation coefficient matrix heatmap of the feature variables and the label

5.2　XGboost

The XGBoost algorithm is a prominent member of the Boosting class in Ensemble learning algorithms[37]. Its approach involves integrating multiple base models, including classification and regression decision trees, as well as linear models, to form a powerful predictive model capable of addressing classification and regression problems. Its underlying principle relies on generating multiple iterations, with each iteration producing a weak classifier. The algorithm then trains on the residuals of the previous round of classifiers to improve the accuracy of subsequent rounds of classifiers. The predictions of all weak classifiers are weighted and combined to yield the result. The prediction process of the XGBoost algorithm for the i-th sample is depicted in Fig. 10.

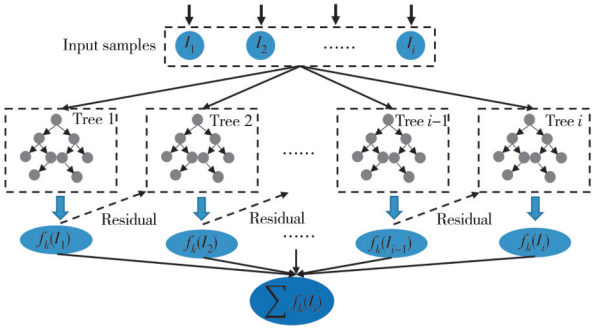

Fig. 10　Structure of XGBoost

In the figure, $\sum f_k(I_i)$ represents the predicted value, and $f_k(I_i)$ denotes the prediction result of the k-th tree for the i-th sample. The process unfolds as follows: for the i-th sample, the predicted value of the first tree is $f_1(I_i)$, and the predicted value of the second tree is $f_2(I_i)$. Subsequently, the predicted values of the total number of K trees are summed together to obtain the final predicted value of the model for the i-th sample.

5.3　ANN

Artificial neural network (ANN) is an information processing technology inspired by the human nervous system, employing interconnected neurons for computations[38]. Through various algorithms, the connection weights and biases between neurons are adjusted based on input data, enabling the network to adapt its structure and predict output. The learning process in ANNs involves training the network on labeled data (supervised learning) or unlabeled data (unsupervised or semi-supervised learning). During training, the network adjusts its connection weights and biases iteratively to minimize the error between the predicted outputs and the true labels (in supervised learning) or to find meaningful patterns in the data (in unsupervised learning). Through backpropagation, the network updates the weights and biases based on the gradient of the cost function with respect to the model's parameters. This optimization process aims to improve the model's performance to generalize new data.

Fig. 11 illustrates this concept, where I_i denotes input layer neurons, J_i and K_i represent different hidden layer neurons, and L_1 indicates output layer neurons. The connection between input and output involves nonlinear relationships. In the diagram, ω_{ij} signifies the weight between the i-th neuron in the input layer and the j-th neuron in the hidden layer, ω_{jk} represents the weight between the j-th neuron in the first hidden layer and the k-th neuron in the second hidden layer, and ω_{kl} denotes the weight between the k-th neuron in the second hidden layer and the l-th neuron in the output layer. F_i represents the transfer function of the hidden layer neuron,

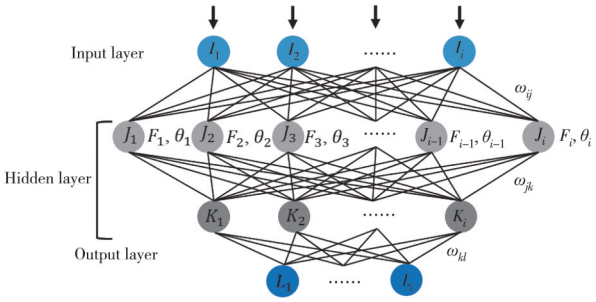

Fig. 11　Structure of artificial neural network

while θ_i denotes the bias of hidden layer neurons.

5.4 Modeling results

The predictive performance of two machine learning methods, XGBoost and Artificial Neural Networks (ANN), is evaluated based on three indicators: Root Mean Squared Error (RMSE), Coefficient of Determination (R^2) and Mean Absolute Percentage Error (MAPE). The evaluation is performed in the context of predicting uplift resistance. Table 3 presents the RMSE, R^2, and MAPE values for the test and training sets using both XGBoost and ANN. The results indicate that XGBoost outperformed ANN in terms of predictive accuracy. For the test set, XGBoost achieves an RMSE of 0.019 and a MAPE of 0.008, while ANN yields slightly higher values of 0.041 and 0.011, respectively. Similarly, for the training set, XGBoost demonstrates superior performance with an RMSE of 0.010 and a MAPE of 0.004, compared to ANN's values of 0.027 and 0.008, respectively. Furthermore, the R^2 values are calculated to assess the goodness of fit of the models (as shown in Fig. 12). XGBoost achieves impressive R^2 values of 0.998 and 0.995 for the training and testing sets, respectively, indicating a high degree of correlation between the predicted and actual uplift resistance.

Table 3 Performance indices for the XGBoost and ANN models

Methods	RMSE		R^2		MAPE	
	Testing	Training	Testing	Training	Testing	Training
XGBoost	0.019	0.010	0.997	0.998	0.008	0.004
ANN	0.041	0.027	0.984	0.995	0.011	0.008

The results highlight the favorable predictive capabilities of XGBoost in accurately forecasting uplift forces in shield tunnels when compared to ANN. This advantage can be attributed to XGBoost's efficient handling of nonlinear relationships between features and target variables through its decision tree-based approach. While ANN is also capable of capturing nonlinear patterns, it often requires a larger number of hidden layers and neurons, making it more susceptible to overfitting and challenging to fine-tune. Moreover, XGBoost provides more interpretable results as it constructs decision trees that can be easily visualized and comprehended. In contrast, the complex architecture of ANN, with multiple hidden layers, renders its learned features and decision-making process harder to interpret. It is essential to acknowledge that the performance of XGBoost and ANN can vary depending on data characteristics, problem complexity, dataset size, and the expertise of the modeler in hyperparameter tuning for each algorithm. As a result, a prudent approach involves exploring both XGBoost and ANN for a specific prob-

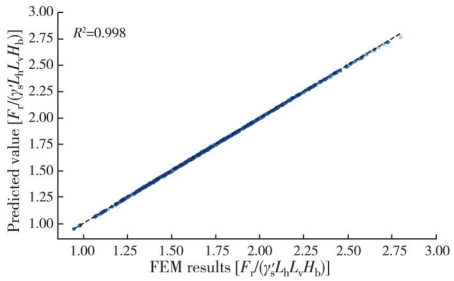

(a) Comparison of the FEM results and the XGBoost results (Training set)

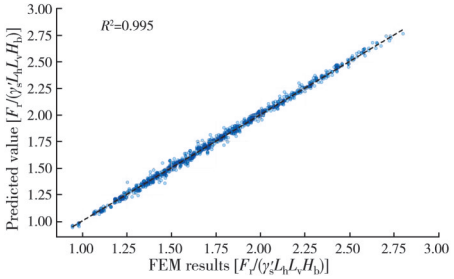

(b) Comparison of the FEM results and the ANN results (Training set)

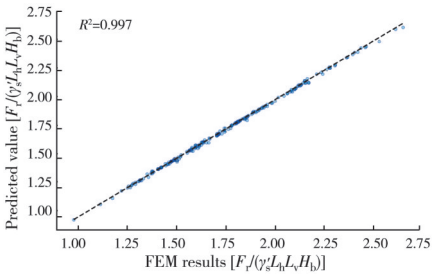

(c) Comparison of the FEM results and the XGBoost results (Testing set)

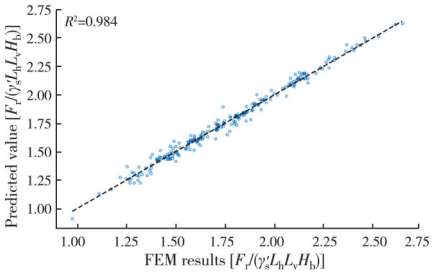

(d) Comparison of the FEM results and the ANN results (Testing set)

Fig. 12 Comparison of XGBoost and ANN prediction performance

lem.

Due to its superior predictive performance, XGBoost is used for parameter importance analysis. As illustrated in Fig. 13, all six parameters exhibit certain impacts on the uplift resistance, with their importance in decreasing order as follows: burial depth ratio (39.67%), internal friction angle (23.91%), maximum horizontal length of the tunnel (12.86%), cohesion (11.50%), tunnel shape coefficient (6.57%), and soil submerged bulk density (5.49%).

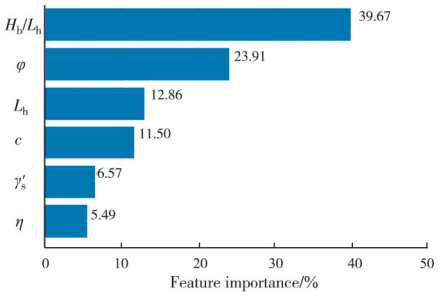

Fig. 13　Feature importance of XGBoost

The burial depth ratio of the tunnel emerges as the most influential factor affecting tunnel anti-floating stability. Under identical geological conditions, an increase in the burial depth ratio implies a corresponding increase in the uplift resistance provided by the overlying soil due to the weight of the soil being a significant component of the uplift resistance. This observation confirms the feasibility of enhancing the anti-floating stability of shield tunnels through the manipulation of tunnel burial depth. The mechanism by which the longest horizontal length and burial depth ratio of a tunnel influence uplift resistance is similar. Both tunnel burial depth and horizontal length affect the range of soil overlying the tunnel that can contribute to uplift resistance. As the horizontal length of the tunnel cross-section increases, the range of soil capable of providing uplift resistance also increases, resulting in greater uplift resistance. Nevertheless, it is essential to consider that an increase in tunnel cross-section also amplifies the upward buoyancy acting on the tunnel. Moreover, the shape coefficient of the tunnel also has an impact on the uplift force. Therefore, the design of tunnel dimensions should strike a balance, considering the impact of tunnel geometry on tunnel stability.

The internal friction angle of the soil, representing the ratio of frictional force between soil particles and the perpendicular pressure at their contact surface. plays a key role in soil mechanics; it significantly influences the soil's stability and bearing capacity. As external forces act upon the soil, the inter-particle friction provides resistance, thus sustaining soil stability. Consequently, a soil layer characterized by a higher internal friction angle contributes to a more substantial uplift resistance from the overlying soil, leading to heightened tunnel stability. Cohesion substantially impacts the shear strength and compressive performance of the soil. During the upward movement of a shield tunnel, cohesion plays a vital role between the overlying and the surrounding soils, forming one of the integral components of uplift resistance. Moreover, the increase in soil submerged bulk density leads to an increase in pressure exerted by the overlying soil on the tunnel.

6　Conclusion

This study employs two approaches involving numerical simulation and machine learning techniques to investigate the uplift resistance of soil above special-shaped shield tunnels. The findings offer valuable insights into the relative significance of these parameters, thereby guiding tunnel design and construction methodologies. The outcomes of this study can be summarized as follows:

(1) The study examines the uplift behavior of shield tunnels during excavation, grouting, and operational stages. It further provides a summarized categorization of existing special-shaped shield tunnels into four primary forms: circular, sub-rectangular, quasi-rectangular, and rectangular.

(2) A novel shape coefficient is introduced to quantify special-shaped shield tunnels. By integrating numerical simulation methods, the impact of this coefficient and five additional parameters (burial depth ratio, longest horizontal length, internal friction angle, cohesion, and soil submerged bulk density) on uplift resistance is systematically analyzed. The findings indicate that tunnel shapes closer to circular exhibit lower uplift resistance in the overlying soil, while uplift resistance increases with higher values of the remaining five parameters.

(3) Numerical simulations using XGBoost and

ANN were performed to assess the influence of various variables on uplift resistance. The results show that XGBoost outperformed ANN in predicting uplift resistance. The parameters' significance is ranked in decreasing order as follows: buried depth ratio, internal friction angle, tunnel longest horizontal length, cohesion, soil submerged bulk density, and shape coefficient.

References

[1] ZHANG X, WANG M N, WANG Z L, et al. A limit equilibrium model for the reinforced face stability analysis of a shallow tunnel in cohesive-frictional soils [J]. Tunnelling and Underground Space Technology, 2020, 105: 103562.

[2] LI J B. Key technologies and applications of the design and manufacturing of non-circular TBMs [J]. Engineering, 2017, 3(6): 905-914.

[3] HUANG X, ZHU Y T, ZHANG Z X, et al. Mechanical behaviour of segmental lining of a sub-rectangular shield tunnel under self-weight [J]. Tunnelling and Underground Space Technology, 2018, 74: 131-144.

[4] ZHU Y T, ZHANG Z X, HUANG X, et al. Exploring the progressive failure characteristics of a large special-shaped shield tunnel lining based on 'standing' prototype loading tests [J]. Tunnelling and Underground Space Technology, 2019, 93: 103107.

[5] PHAM V V, DO N A, DIAS D. Sub-rectangular tunnel behavior under seismic loading [J]. Applied Sciences, 2021, 11(21): 9909.

[6] DO N A, DIAS D, ZHANG Z X, et al. Study on the behavior of squared and sub-rectangular tunnels using the Hyperstatic Reaction Method [J]. Transportation Geotechnics, 2020, 22: 100321.

[7] LIU X, YE Y H, LIU Z, et al. Mechanical behavior of quasi-rectangular segmental tunnel linings: First results from full-scale ring tests [J]. Tunnelling and Underground Space Technology, 2018, 71: 440-453.

[8] LI P N, DAI Z Y, HUANG D Z, et al. Impact analysis for safety prevention and control of special-shaped shield construction closely crossing multiple operational metro tunnels in shallow overburden [J]. Geotechnical and Geological Engineering, 2022, 40(4): 2127-2144.

[9] LIU J, LI P N, SHI L, et al. Spatial distribution model of the filling and diffusion pressure of synchronous grouting in a quasi-rectangular shield and its experimental verification [J]. Underground Space, 2021, 6(6): 650-664.

[10] DING W Q, DUAN C, ZHU Y H, et al. The behavior of synchronous grouting in a quasi-rectangular shield tunnel based on a large visualized model test [J]. Tunnelling and Underground Space Technology, 2019, 83: 409-424.

[11] CHEN X S, SHEN J, BAO X H, et al. A review of seismic resilience of shield tunnels [J]. Tunnelling and Underground Space Technology, 2023, 136: 105075.

[12] NAKAMURA H, KUBOTA T, FURUKAWA M, et al. Unified construction of running track tunnel and cross-over tunnel for subway by rectangular shape double track cross-section shield machine [J]. Tunnelling and Underground Space Technology, 2003, 18(2/3): 253-262.

[13] VINOD M, KHABBAZ H. Comparison of rectangular and circular bored twin tunnels in weak ground [J]. Underground Space, 2019, 4(4): 328-339.

[14] CHEN X L, MA B S, NAJAFI M, et al. Long rectangular box jacking project: A case study [J]. Underground Space, 2021, 6(2): 101-125.

[15] LI P F, LIU H C, ZHAO Y, et al. A bottom-to-up drainage and water pressure reduction system for railway tunnels [J]. Tunnelling and Underground Space Technology, 2018, 81: 296-305.

[16] MAO J H, YUAN D J, JIN D L, et al. Optimization and application of backfill grouting material for submarine tunnel [J]. Construction and Building Materials, 2020, 265: 120281.

[17] GUO C X, QI J, SHI L L, et al. Reasonable overburden thickness for underwater shield tunnel [J]. Tunnelling and Underground Space Technology, 2018, 81: 35-40.

[18] GUO P P, GONG X N, WANG Y X, et al. Minimum cover depth estimation for underwater shield tunnels [J]. Tunnelling and Underground Space Technology, 2021, 115: 104027.

[19] WHITE D J, BAREFOOT A J, BOLTON M D. Centrifuge modelling of upheaval buckling in sand [J]. International Journal of Physical Modelling in Geotechnics, 2001, 1(2): 19-28.

[20] WHITE D J, CHEUK C Y, BOLTON M D. The uplift resistance of pipes and plate anchors buried in sand [J]. Géotechnique, 2008, 58(10): 771-779.

[21] GONG Q M, ZHAO Y, ZHOU J H, et al. Uplift resistance and progressive failure mechanisms of metro shield tunnel in soft clay [J]. Tunnelling and Underground Space Technology, 2018, 82: 222-234.

[22] ROBERT D J, THUSYANTHAN N I. Uplift resistance of buried pipelines in partially saturated sands [J]. Computers and Geotechnics, 2018, 97: 7-19.

[23] LIU X Y, YUAN D J. Mechanical analysis of anti-buoyancy safety for a shield tunnel under water in sands [J]. Tunnelling and Underground Space Technology, 2015, 47: 153-161.

[24] ZHANG W G, PHOON K K. Editorial for Advances

and applications of deep learning and soft computing in geotechnical underground engineering [J]. Journal of Rock Mechanics and Geotechnical Engineering, 2022, 14(3): 671-673.

[25] ZHENG G, ZHANG W B, ZHANG W G, et al. Neural network and support vector machine models for the prediction of the liquefaction-induced uplift displacement of tunnels [J]. Underground Space, 2021, 6(2): 126-133.

[26] ZHANG W G, ZHANG R H, WU C Z, et al. Assessment of basal heave stability for braced excavations in anisotropic clay using extreme gradient boosting and random forest regression [J]. Underground Space, 2022, 7(2): 233-241.

[27] ZHANG W G, WU C Z, ZHONG H Y, et al. Prediction of undrained shear strength using extreme gradient boosting and random forest based on Bayesian optimization [J]. Geoscience Frontiers, 2021, 12(1): 469-477.

[28] LIU S L, WANG L Q, ZHANG W G, et al. A comprehensive review of machine learning-based methods in landslide susceptibility mapping [J]. Geological Journal, 2023, 58(6): 2283-2301.

[29] LIU S L, WANG L Q, ZHANG W G, et al. A physics-informed data-driven model for landslide susceptibility assessment in the Three Gorges Reservoir Area [J]. Geoscience Frontiers, 2023, 14(5): 101621.

[30] WEI G, HONG J, WEI X J. Mechanical analysis of segment floating during shield tunnel construction [J]. Chinese Journal of Rock Mechanics and Engineering, 2012, 31(6): 1257-1263.

[31] VERMEER P A, SUTJIADI W. The uplift resistance of shallow embedded anchors [C]//Proceedings of the Eleventh International Conference on Soil Mechanics and Foundation Engineering: San Francisco, 12-16 August 1985: 1635-1638.

[32] SCHAMINÉE P, ZORN N, SCHOTMAN G J M. Soil response for pipeline upheaval buckling analyses: Full-scale laboratory tests and modelling [C]//Proceedings of the 22nd Annual Offshore Technology Conference, Houston, Texas, May 1990, OTC-6486-MS: 563-572.

[33] NEWSON T, STONE K. Uplift resistance of buried pipelines: An investigation of scale effects in model tests [C]// Proceedings of the Sixth International Conference on Physical Modelling in Geotechnics, Hong Kong, 2006.

[34] PALMER A C, WHITE D J, BAUMGARD A J, et al. Uplift resistance of buried submarine pipelines: Comparison between centrifuge modelling and full-scale tests [J]. Géotechnique, 2003, 53(10): 877-883.

[35] MAGDA W, MAENO S, NAGO H. Floatation of buried submarine pipeline under cyclic loading of water pressure: Numerical and experimental studies [J]. Journal of the Faculty of Environmental Science and Technology, Okayama University, 2000, 5(1): 81-98.

[36] SUN W X, HAN F C, LIU H L, et al. Determination of minimum overburden depth for underwater shield tunnel in sands: Comparison between circular and rectangular tunnels [J]. Journal of Rock Mechanics and Geotechnical Engineering, 2023, 15(7): 1671-1686.

[37] CHEN T Q, GUESTRIN C. XGBoost: A scalable tree boosting system [C]//Proceedings of the 22nd ACM SIGKDD International Conference on Knowledge Discovery and Data Mining. August 13-17, 2016, San Francisco, California, USA. ACM, 2016: 785-794.

[38] ZHANG W G, GOH A T C. Multivariate adaptive regression splines and neural network models for prediction of pile drivability [J]. Geoscience Frontiers, 2016, 7(1): 45-52.

（编辑　胡英奎）